RETRIEVAL OF THE BACKSCATTER CROSS-SECTION IN FULL-WAVEFORM LIDAR DATA USING B-SPLINES

A. Roncat[a, *], G. Bergauer[b], N. Pfeifer[a]

[a] Institute of Photogrammetry and Remote Sensing (IPF), Vienna University of Technology, Austria – (ar,np)@ipf.tuwien.ac.at
[b] Institute of Analysis and Scientific Computing, Vienna University of Technology, Austria – gunther@bergauer.it

Commission III – WG III/2

KEY WORDS: LIDAR, Full-Waveform, Deconvolution

ABSTRACT:

Full-waveform lidar systems transmit short laser pulses towards the Earth's surface and record the complete backscattered echo. This technique does not only allow for the three-dimensional reconstruction of the terrain, natural and man-made objects, but also for the derivation of (geo-)physical parameters such as the (differential) backscatter cross-section. To retrieve this quantity, deconvolution is necessary which is an ill-posed problem. This paper presents a novel technique for the computation of the backscatter cross-section using B-splines which allow for a well-posed linear approach for deconvolution without regularization. Moreover, it is independent on symmetry of the temporal shapes of the emitted laser pulse and the recorded echo waveform, respectively. In this study, the algorithm for deconvolution is described in detail and validated by both synthetic and real full-waveform lidar data.

1 INTRODUCTION

The acquisition of three-dimensional data for topographic purposes has been revolutionized by lidar (Light detection and ranging) in the last 15 years. This technique is also known as laser scanning and allows for the direct observation of spatial coordinates by recording the round-trip time of the echo of the emitted laser pulse and the deflection angles. In contrast to this, in passive imaging only two coordinates can be observed at the same time. Moreover, since it is an active technique, lidar is not dependent on illumination. Most of the current operating lidar systems allow for the recording of multiple echoes per laser shot, thus "seeing through" the foliage is possible to a certain amount, i.e. in vegetated areas.

There exist both airborne (commonly known as airborne laser scanners, ALS) and ground-based (terrestrial laser scanners, TLS) lidar systems. The latest generation of ALS instruments does not record a discrete number of echoes per laser shot, but the sampled copy of the emitted laser pulse as well as the echo waveform. The quantity summarizing the (geo-)physical properties of a target hit by the laser beam is the backscatter cross-section $\sigma(t)$. Its calculation requires deconvolution which is an ill-posed problem.

Section 2 presents the underlying physical model and existing methods for the retrieval of the backscatter cross-section. Our approach for this task is presented in Section 3. In the subsequent section, we illustrate the feasibility of our method by means of both synthetic examples and real lidar data. The paper concludes with the discussion of our results in Section 5.

2 RELATED WORK

2.1 Radar Equation and Backscatter Cross-Section

The radar equation which is applicable to signals in the optical and microwave spectrum equally, relates the emitted power P_E to the received power at the detector P_D (Jelalian, 1992):

$$P_D = \frac{P_E}{\beta_E^2 R^2} \frac{\sigma}{4\pi R^2} \frac{\pi D^2}{4} \eta_{\mathrm{ATM}} \eta_{\mathrm{SYS}} \tag{1}$$

Here β_E is the beamwidth of the emitted signal, R is the range from the sensor to the target, σ is the effective backscatter cross-section (in m^2), D is the aperture diameter, η_{ATM} is the atmospheric transmission factor, and η_{SYS} the system transmission factor. The backscatter cross-section is a product of the target area ($\mathrm{d}A[\mathrm{m}^2]$), the target reflectivity ($\rho[\,]$), and the factor $4\pi/\Omega$ describing the scattering angle of the target ($\Omega[\mathrm{sr}]$) in relation to an isotropic scatterer (Jelalian, 1992):

$$\sigma = \frac{4\pi}{\Omega} \rho \, \mathrm{d}A \tag{2}$$

If the area upon which the signal is reflected is larger than the laser's footprint, the target area becomes proportional to the square of the range, reducing the $1/R^4$ relation in Equation (1) to $1/R^2$.

In the above it is assumed that the target is a flat face orthogonal to the beam. A more detailed analysis, presented by (Wagner et al., 2006) includes the temporal shape of the emitted signal $P_E(t)$ and the spatial distribution of the targets along the laser beam $\sigma_i(R)$, i.e. the differential backscatter cross-section. The target cross-section is the integral of the target's backscatter cross-section. With some simplifications and omission of the transmission factors of Equation (1) this leads to:

$$P_{D,i}(t) \approx \frac{D^2}{4\pi R_i^4 \beta_E^2} \int_{R_i-\delta}^{R_i+\delta} P_E\left(t - \frac{2R}{v_g}\right) \sigma_i(R) \, \mathrm{d}R \tag{3}$$

Here, v_g is the group velocity of the laser ray, and each differential backscatter cross-section σ_i is within the interval $[R_i - \delta, R_i + \delta]$. Equation (3) includes the convolution of the emitted laser pulse with the differential backscatter cross-section of the target, leading to the backscattered waveform. In full-waveform laser scanning, this waveform is recorded by sampling it. Operational airborne systems typically use a sampling interval of 1 ns (Wagner et al., 2006).

The transmitted waveform might be unknown, whereas the output of the detector when receiving the transmitted waveform can be recorded. This waveform is called the system waveform and may be used instead of $P_E(t)$ in Equation (3).

* Corresponding author.

2.2 Existing Approaches

A number of methods has been published for analysing recorded waveforms, e.g for decomposing the waveform into Gaussian (Duong et al., 2008; Wagner et al., 2006; Hofton et al., 2000) or more complex (Mallet et al., 2009) components. The parameters of these components can then be compared from one epoch to another or related to other observations, e.g. land cover (Duong et al., 2009) or forest parameters (Lefsky et al., 2002). These methods do not extract parameters of the scattering surface, but quantities that are also influenced by mission parameters. Thus, the values are not comparable for laser scanners operating with, e.g., different lengths of the emitted pulses.

In (Wagner et al., 2006) the backscatter cross-section is determined. In this approach it is assumed that the the temporal shape of the emitted pulse is Gaussian as well as the scatterers' differential backscatter cross-section Since the convolution of two Gaussians again yields a Gaussian, the recorded echo results in a Gaussian, too. The variance of the backscattered waveform is the sum of the variances of the emitted pulse and the differential backscatter cross-section of the target. The last sentence comprises the deconvolution implicitly.

The algorithm presented in (Jutzi and Stilla, 2006) comprises the transformation of the emitted pulse and the received waveform to the frequency domain. Thus, the differential backscatter cross-section is retrieved as the result of division of the spectrum of the received waveform by the spectrum of the emitted pulse. In this approach, a Wiener Filter is applied for noise reduction in the frequency domain.

In (Wang et al., 2009), an approach for discrete deconvolution in the time domain is proposed. The emitted pulse, the received echo, and the differential backscatter cross-sections are treated as continuous, piecewise linear functions. Rewriting the deconvolution as a system of linear equations becomes thus possible. Regularization is used to gain numerical stability in the solution and to handle noise.

3 METHOD

3.1 Uniform B-Spline Curves

A uniform B-Spline $B_l^n(u)$ is a piecewise continuous function of degree n (C^{n-1} continuity). It is recursively defined by repeated convolution (Zorin and Schröder, 2000):

$$B_l^n(u) = B_l^{n-1}(u) \otimes B_1^0(u) = \int_{-\infty}^{\infty} B_1^{n-1}(\tau) B_1^0(u-\tau)\,\mathrm{d}\tau \quad (4)$$

starting with

$$B_l^0(u) = \begin{cases} 1 & \dots (l-1)\Delta u \le u < l\Delta u \\ 0 & \dots \text{ elsewhere} \end{cases}$$

where $\Delta u = \text{const}$. The $B_l^n(u)$ are positive within the interval $((l-1)\Delta u, (l+n)\Delta u)$ and strictly zero outside (Zorin and Schröder, 2000; Farin, 2002). Without loss of generality, we can set $\Delta u = 1$. Equation (4) may be rewritten as

$$B_l^n(u) = B_k^m(u) \otimes B_{l-k+1}^{n-m+1}(u) \quad (5)$$

Figure 1 illustrates the construction of uniform B-splines of degree 0 to 2.

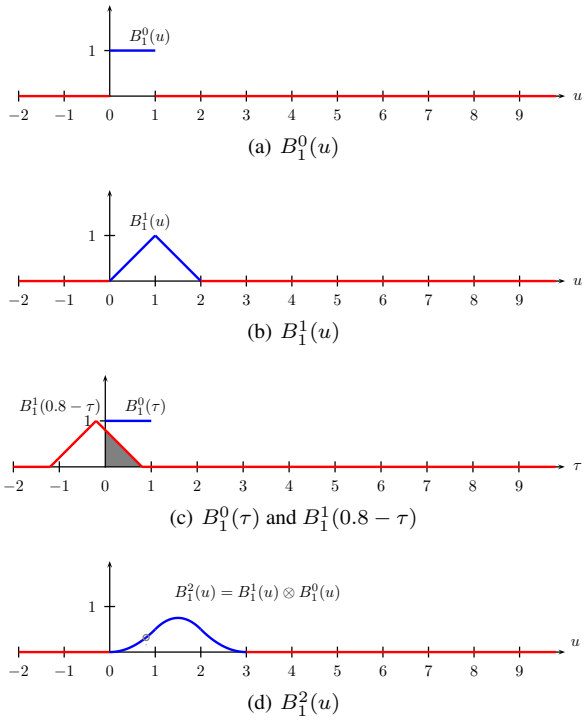

(a) $B_1^0(u)$ (b) $B_1^1(u)$ (c) $B_1^0(\tau)$ and $B_1^1(0.8-\tau)$ (d) $B_1^2(u)$

Figure 1: Uniform B-splines of degree 0 (a) and 1 (b). Image (c) illustrates the construction of the uniform B-spline of degree 2, $B_1^2(u)$, as the result of the convolution $B_1^0(u) \otimes B_1^1(u)$; the gray-hatched area is equal to the integral $\int B_1^0(\tau)\, B_1^0(0.8-\tau)\,\mathrm{d}\tau$ and therefore to $B_1^2(0.8)$. $B_1^2(u)$ itself is shown in (d), $B_1^2(0.8)$ is indicated by the gray circle.

A uniform B-spline curve $\gamma(u) = (\gamma_1(u), \dots, \gamma_m(u))^\top \subset \mathbb{R}^m$ of degree n is defined as a linear combination of uniform B-splines

$$\gamma(u) = \sum_{i=1}^{i_{\max}} \mathbf{b}_i B_i^n(u) \quad (6)$$

with the $\mathbf{b}_i$ forming the control polygon. Fitting a B-spline curve to observations is a linear least-squares problem

$$\sum_{j=1}^{j_{\max}} \left(y(u_j) - \sum_{i=1}^{i_{\max}} \mathbf{b}_i B_i^n(u_j) \right)^2 \to \min. \quad (7)$$

In the case of full-waveform lidar, the $y(u_j)$ denote the observed amplitude values of the recorded waveform at time u_j and the $\mathbf{b}_i$ denote the unknown control points which are one-dimensional in our case, i.e. $\mathbf{b}_i = b_i$.

3.2 Convolution and Deconvolution of B-Spline Curves

Suppose we have already determined the uniform B-spline curve representation for reference pulse ($\rho(u)$) and differential backscatter cross-section ($\kappa(u)$) of degree n_{rp} and n_{cs}, respectively:

$$\rho(u) := \sum_{i=1}^{i_{\max}} b_{i,\text{rp}} B_i^{n_{\text{rp}}}(u), \quad \kappa(u) := \sum_{j=1}^{j_{\max}} b_{j,\text{cs}} B_j^{n_{\text{cs}}}(u) \quad (8)$$

We can now write the uniform B-spline curve representing the echo waveform, $\omega(u)$ as the result of the convolution of the two

curves given above, making use of Equation (5):

$$\begin{aligned}\omega(u) &:= \sum_{k=1}^{k_{\max}=i_{\max}+j_{\max}-1} b_{k,\mathrm{wf}} B_k^{n_{\mathrm{wf}}}(u) \\ &= \sum_{i=1}^{i_{\max}} \sum_{j=1}^{j_{\max}} \left(b_{i,\mathrm{rp}} B_i^{n_{\mathrm{rp}}}(u)\right) \otimes \left(b_{j,\mathrm{cs}} B_j^{n_{\mathrm{cs}}}(u)\right) \\ &= \sum_{i=1}^{i_{\max}} \sum_{j=1}^{j_{\max}} (b_{i,\mathrm{rp}} b_{j,\mathrm{cs}}) \underbrace{\left(B_i^{n_{\mathrm{rp}}}(u) \otimes B_j^{n_{\mathrm{cs}}}(u)\right)}_{B_{i+j-1}^{n_{\mathrm{rp}}+n_{\mathrm{cs}}+1}=B_{i+j-1}^{n_{\mathrm{wf}}}}\end{aligned} \tag{9}$$

The control points of $\omega(u)$ are therefore

$$b_{k,\mathrm{wf}} = \sum_{i,j:i+j-1=k} b_{i,\mathrm{rp}} b_{j,\mathrm{cs}}$$

In the case of full-waveform lidar, the $b_{i,\mathrm{rp}}$ and $b_{k,\mathrm{wf}}$ can be easily determined by least-squares curve fitting (see Equation (7)) whereas the $b_{j,\mathrm{cs}}$ remain preliminarily unknown. Thus, the equation given above may be taken as an observation equation in a least-squares approach for deconvolution. Its set-up is linear in the parameters $b_{j,\mathrm{cs}}$ and can therefore be solved in one iteration without knowing approximate values.

4 EXAMPLES

In this section, we deliver empirical evidence for the success of our deconvolution approach on behalf of synthetic waveform data (Section 4.1) and real data of an ALS campaign (Section 4.2).

4.1 Synthetic Example

First, a synthetic example is given, comprising the reference pulse and the differential backscatter cross-section. Both of them are of degree 3, leading to the backscattered waveform by convolution with degree 7. For our examples, the amplitudes were normalized in the form that the value of the respectively greatest $b_{i,\mathrm{rp}}$ and $b_{j,\mathrm{cs}}$ was set to 1. The reference pulse has a slightly asymmetrical temporal shape (see Figure 2(a)). Its control polygon consists of three significant (i.e. non-zero) vertices so that the whole reference pulse has a duration of 7 ns. The full width at half maximum (FWHM) of this pulse is 1.8 ns.

For the reconstruction of the differential backscatter cross-section, both the synthetic reference pulse and the synthetic waveform were sampled in 1 ns intervals. To test the stability of our algorithm in the presence of noise, we applied four sampling variants:

- noise-free ("×" markers in Figure 2)
- added Gaussian noise with $\sigma = 0.01$ ("+" markers)
- added Gaussian noise with $\sigma = 0.02$ ("·" markers)
- added Gaussian noise with $\sigma = 0.05$ ("○" markers)

To assess the performance of our approach, we analysed the square root of the variance a posteriori of the deconvolution, s_0. Furthermore, the root mean square error, r.m.s. and on the normalized root mean square error, $\mathrm{r.m.s._{norm}}$ of both the curve fits and the deconvolution were investigated, too (see Table 1). The definition of the last two is given as follows:

$$\mathrm{r.m.s.}(f(u), g(u)) := \sqrt{\frac{1}{u_{\max} - u_{\min}} \int_{u_{\min}}^{u_{\max}} (f(u) - g(u))^2 \, \mathrm{d}u}$$

and

$$\mathrm{r.m.s._{norm}}(f(u), g(u)) := \frac{\mathrm{r.m.s.}(f(u), g(u))}{\mathrm{r.m.s.}(g(u), 0)}$$

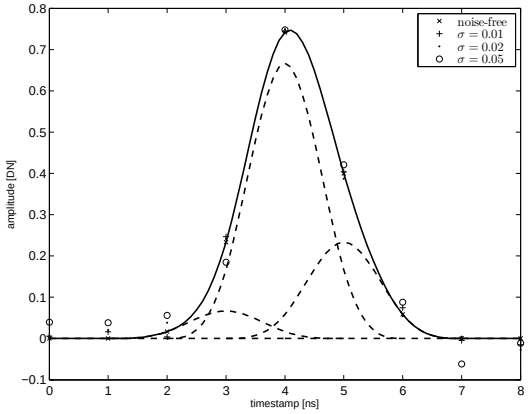

(a) Synthetic laser pulse $\rho(u)$

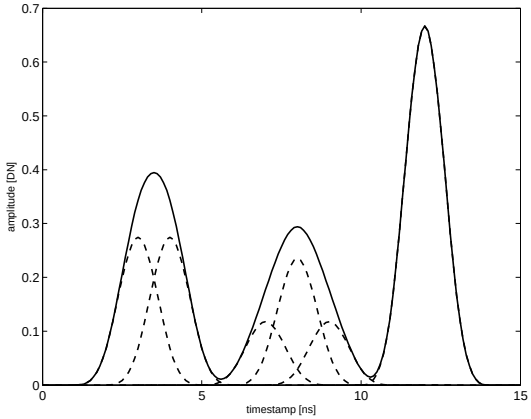

(b) Differential backscatter cross-section representing three symmetric scatterers $\kappa(u)$

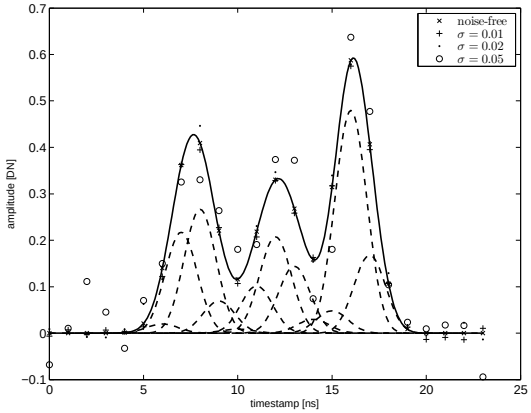

(c) Synthetic waveform as result of the convolution of 2(a) and 2(b)

Figure 2: Construction of a synthetic example for B-spline convolution. B-splines are shown as solid lines, while their individual components are dashed curves. Images (a) and (b) show the emitted pulse and the differential backscatter cross-section of three symmetric scatterers, resp. In (c), the echo waveform corresponding to these data is shown. "×", "+", "·" and "○" markers indicate sampled values without and with added Gaussian noise of different intensity.

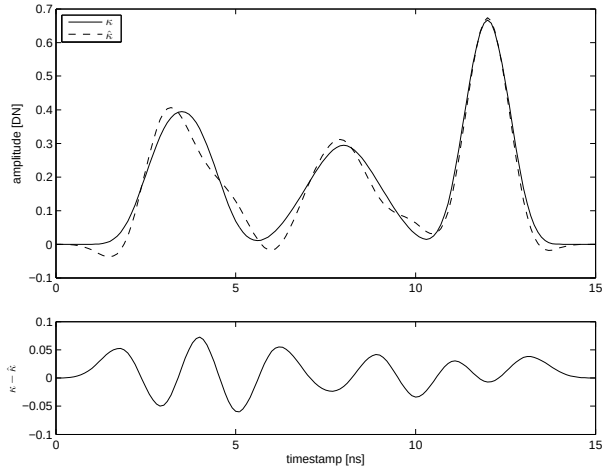

Figure 3: Top: Synthetic ($\kappa(u)$, solid line) vs. reconstructed differential backscatter cross-section ($\hat{\kappa}(u)$, dashed line), noise level $\sigma = 0.01$. Bottom: Difference $\kappa(u) - \hat{\kappa}(u)$ of the two curves.

resp. In the examples treated here, $u_{\min}$ is always equal to 0 and $u_{\max}$ is equal to $\Delta u\, i_{\max}$, $\Delta u\, j_{\max}$ or $\Delta u\, k_{\max}$, resp.

In the case of error-free sampling, the reconstruction of the synthetic waveform was possible without any noticeable error. This is valid for the deconvolution, too. With increasing noise, the s_0 got higher according to the noise level, as well as the r.m.s. errors.

noise level (σ), symbol	s_0	r.m.s. $(\bar{\kappa}(u), \kappa(u))$	$\text{r.m.s.}_{\text{norm}}$ $(\bar{\kappa}(u), \kappa(u))$
0 ($\times$)	0.0000	0.0000	0.0000
0.01 ($+$)	0.0543	0.0306	0.1270
0.02 ($\cdot$)	0.0978	0.0463	0.1919
0.05 ($\circ$)	0.1035	0.0980	0.4066

Table 1: Deconvolution error analysis of of the synthetic example

4.2 Examples of Real Lidar Waveforms

The lidar waveforms shown in Figure 4 were acquired during a flight mission in early 2007 in the Leithagebirge (Burgenland, Eastern Austria (Doneus et al., 2008)). The example comprises 16 subsequent laser pulses and their echo waveforms which were sampled by the instrument, a Riegl LMS-Q560 airborne lidar system (Riegl, 2010), in 1 ns intervals each. As visible in Figure 4(b), our sample contains single narrow echoes with high amplitudes (e.g. laser pulse 2740371 and 2740372) as well as multimodal waveforms with overlapping scatterers (e.g. laser pulses 2740370 and 2740377). Analogously to the synthetic examples, the reference pulses were approximated as B-spline curves of degree 3 and a control point spacing of 2 ns. The echo waveforms were modeled as B-Spline curves of degree 7 and the same control point spacing. Thus, the differential backscatter cross-section results in B-spline curves of degree 3 with the same distance of the control points.

Figure 4(c) shows the results of our deconvolution approach. For the whole sample, both B-spline curve fitting and deconvolution yield sensible results. However, the s_0 a posteriori of the deconvolution varies significantly (see Figure 5). One possible reason for this might be the that the vertices of the reference pulse's control polygon $b_{i,\text{rp}}$ are treated as constants in the adjustment and their stochastic properties are therefore neglected.

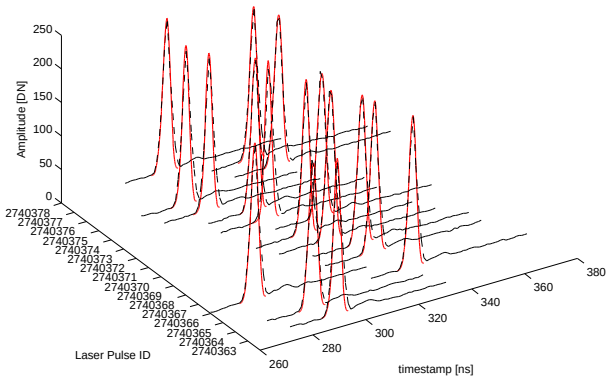

(a) Sampled reference pulses (black) and their B-Spline approximations (red)

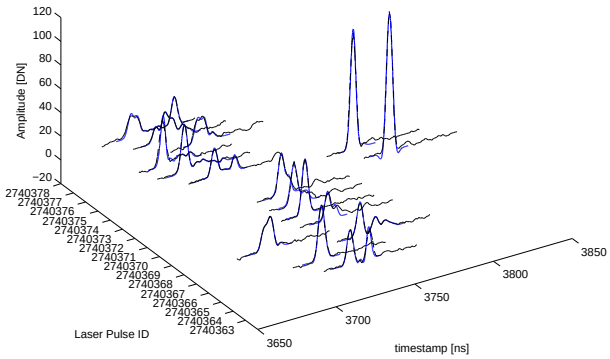

(b) Sampled echo waveforms (black) and their B-Spline approximations (blue)

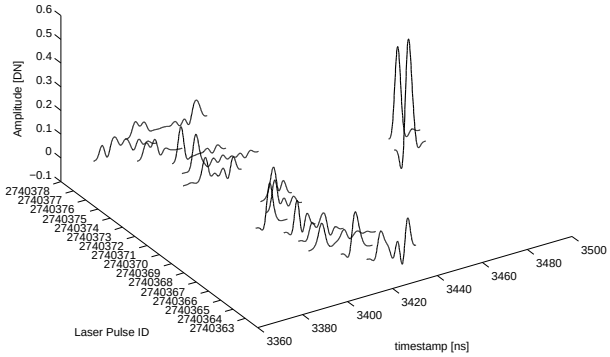

(c) Differential backscatter cross-sections retrieved by B-Spline-based deconvolution

Figure 4: Examples for B-Spline approximation and deconvolution of 16 subsequent laser pulses and their echo waveforms

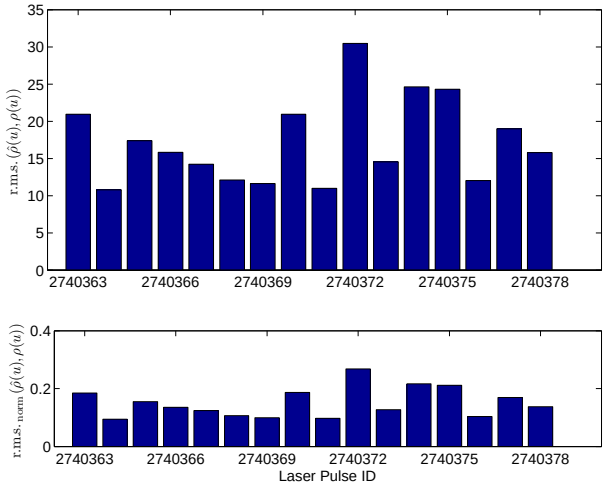

(a) r.m.s. values for curve fitting of Reference Pulses

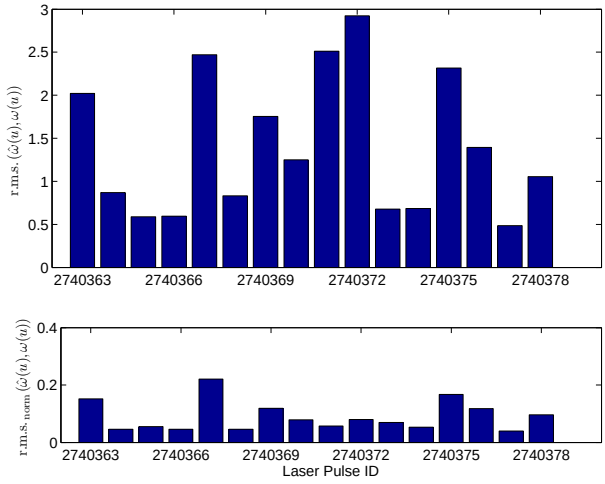

(b) r.m.s. values for curve fitting of Echo Waveforms

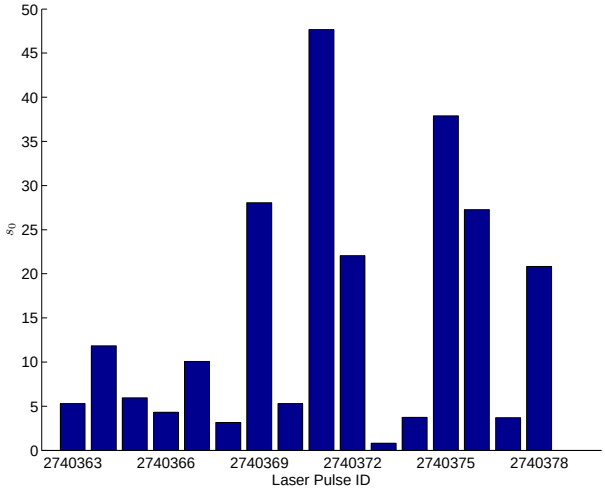

(c) s_0 of deconvolution

Figure 5: Error analysis of B-spline curve fitting ((a) and (b)) and deconvolution (c)

This bias could be overcome by setting up a overall model following the general case for adjustment (Mikhail, 1976) with the already determined parameters serving as initial values for the unknowns. This model contains the recorded sampled values of reference pulse and echo waveform as observations and the convolution equations in the scheme of Equation (9) as constraints.

5 DISCUSSION AND OUTLOOK

In this study, we presented a novel approach for the derivation of the differential backscatter cross-section in full-waveform lidar data. The technique is based on the use of uniform B-splines for modeling the curves representing the emitted laser pulse and the recorded echo waveform as well as for performing the actual computation of the differential cross-section. This implies deconvolution which is an ill-posed problem itself. However, uniform B-splines enable for solving the deconvolution in a linear least-squares approach.

The feasibility of our approach was tested on behalf of both synthetic and real waveform data. The algorithm performed well in all investigated cases. The actual deconvolution is indeed biased by introducing already determined parameters as constants and neglecting their stochastic properties. This drawback can be overcome by the set-up of an overall adjustment following the general case for adjustment.

Another important issue is the occurrence of negative amplitudes in the deconvolved differential backscatter cross-section. These negative values may appear when the signal strength of the backscattered echo is low in comparison to the noise level (Mücke, 2008). In this case, the echo waveforms may be narrower than the emitted laser pulse, causing negative amplitudes in B-spline deconvolution or imaginary results in Gaussian decomposition. However, both are physically meaningless and ought therefore to be ruled out. The determination of the next-best solution compliant with the physical model is currently under investigation.

ACKNOWLEDGEMENTS

We would like to thank Wolfgang Wagner, Josef Jansa, Helmut Kager, Thomas Melzer (all IPF) and Andreas Ullrich (Riegl Laser Measurement Systems) for the interesting discussions and their helpful suggestions.

The ALS data acquisition in the Leithagebirge was part of the research projects “Celts in the Hinterland of Carnuntum” and “LiDAR supported archaeological prospection of woodland” which were financed by the Austrian Science Fund (P16449-G02; P18674-G02).

References

Doneus, M., Briese, C., Fera, M. and Janner, M., 2008. Archaeological prospection of forested areas using full-waveform airborne laser scanning. Journal of Archaeological Science 35(4), pp. 882–893.

Duong, H. V., Lindenbergh, R., Pfeifer, N. and Vosselman, G., 2008. Single and two epoch analysis of icesat full waveform data over forested areas. International Journal of Remote Sensing 29(5), pp. 1453–1473.

Duong, H. V., Lindenbergh, R., Pfeifer, N. and Vosselman, G., 2009. Icesat full waveform altimetry compared to airborne laser scanning altimetry over the netherlands. IEEE Transactions on Geoscience and Remote Sensing 47(10), pp. 3365–3378.

Farin, G., 2002. Curves and Surfaces for CAGD. A Practical Guide. 5th edn, Morgan Kaufmann Publishers, San Francisco, USA.

Hofton, M., Minster, J. and Blair, J., 2000. Decomposition of laser altimeter waveforms. IEEE Transactions on Geoscience and Remote Sensing 38, pp. 1989–1996.

Jelalian, A. V., 1992. Laser Radar Systems. Artech House, Boston.

Jutzi, B. and Stilla, U., 2006. Range determination with waveform recording laser systems using a wiener filter. ISPRS Journal of Photogrammetry and Remote Sensing 61(1), pp. 95–107.

Lefsky, M. A., Cohen, W. B., Parker, G. G. and Harding, D. J., 2002. Lidar remote sensing for ecosystem studies. BioScience 52(1), pp. 19–30.

Mallet, C., Lafarge, F., Bretar, F., Roux, M., Soergel, U. and Heipke, C., 2009. A stochastic approach for modelling airborne lidar waveforms. In: F. Bretar, M. Pierrot-Deseilligny and G. Vosselman (eds), Laserscanning 2009 – International Archives of the Photogrammetry, Remote Sensing and Spatial Information Sciences XXXVIII, Part 3/W8, pp. 201–206.

Mikhail, E. M., 1976. Observations And Least Squares. IEP-A Dun-Donnelley, New York.

Mücke, W., 2008. Analysis of full-waveform airborne laser scanning data for the improvement of DTM generation. Master's thesis, Institute of Photogrammetry and Remote Sensing, Vienna University of Technology.

Riegl, 2010. www.riegl.com. Homepage of the company RIEGL Laser Measurement Systems GmbH, accessed: April 2010.

Wagner, W., Ullrich, A., Ducic, V., Melzer, T. and Studnicka, N., 2006. Gaussian decomposition and calibration of a novel small-footprint full-waveform digitising airborne laser scanner. ISPRS Journal of Photogrammetry and Remote Sensing 60(2), pp. 100–112.

Wang, Y., Zhang, J., Roncat, A., Künzer, C. and Wagner, W., 2009. Regularizing method for the determination of the backscatter cross section in lidar data. Journal of the Optical Society of America A 26(5), pp. 1071–1079.

Zorin, D. and Schröder, P., 2000. Subdivision for modeling and animation. SIGGRAPH 2000 Course Notes. http://www.multires.caltech.edu/pubs/pubs.htm.